Nuclear Engineering and Technology 55 (2023) 3359–3366

Contents lists available at ScienceDirect

Nuclear Engineering and Technology

journal homepage: www.elsevier.com/locate/net

Original Article

Discrimination of neutrons and gamma-rays in plastic scintillator based on spiking cortical model☆

Bing-Qi Liu [a, b, *], Hao-Ran Liu [b, c], Lan Chang [c, d], Yu-Xin Cheng [c], Zhuo Zuo [b, c, d], Peng Li [c]

[a] Chengdu University, Chengdu, 610106, China
[b] State Key Laboratory of Geohazard Prevention and Geoenvironment Protection, Chengdu University of Technology, Chengdu, 610059, China
[c] The Engineering & Technical College of Chengdu University of Technology, Leshan, 614000, China
[d] Southwestern Institute of Physics, Chengdu, 610225, China

ARTICLE INFO

Article history:
Received 13 March 2022
Received in revised form
11 April 2023
Accepted 20 April 2023
Available online 26 June 2023

Keywords:
Spiking cortical model
Pulse shape discrimination
Neutron and gamma-ray discrimination
Charge comparison
Feature extraction

ABSTRACT

In this study, a spiking cortical model (SCM) based n-γ discrimination method is proposed. The SCM-based algorithm is compared with three other methods, namely: (i) the pulse-coupled neural network (PCNN), (ii) the charge comparison, and (iii) the zero-crossing. The objective evaluation criteria used for the comparison are the *FoM*-value and the time consumption of discrimination. Experimental results demonstrated that our proposed method outperforms the other methods significantly with the highest *FoM*-value. Specifically, the proposed method exhibits a 34.81% improvement compared with the PCNN, a 50.29% improvement compared with the charge comparison, and a 110.02% improvement compared with the zero-crossing. Additionally, the proposed method features the second-fastest discrimination time, where it is 75.67% faster than the PCNN, 70.65% faster than the charge comparison and 38.4% slower than the zero-crossing. Our study also discusses the role and change pattern of each parameter of the SCM to guide the selection process. It concludes that the SCM's outstanding ability to recognize the dynamic information in the pulse signal, improved accuracy when compared to the PCNN, and better computational complexity enables the SCM to exhibit excellent n-γ discrimination performance while consuming less time.

1. Introduction

The neutron detection technique is a critical component of many modern industrial areas, such as reactors [1], medical imaging [2], geography [3], irradiation facilities [4] and the aerospace industry [5]. However, capturing neutron signals is challenging for quite a long time due to the accompanying gamma-rays resulting from the interaction between neutrons and their surroundings. Radiation detectors, when deployed to detect neutrons, capture n-γ pulse signals simultaneously, making it challenging to distinguish whether the radiation signal counts originate from neutrons or gamma-rays. To address this challenge, Brooks [6] discovered an intrinsic difference in the shapes of n-γ pulse signals retrieved by organic detectors. This difference makes it possible to discriminate neutrons and gamma-rays by their pulse signals. This discovery led to the development of pulse shape discrimination (PSD) [7,8], various detectors that can work in different situations have been developed [9,10], and many discrimination methods of neutrons and gamma-rays have been proposed like zero-crossing method [11], charge comparison method [12] and falling edge percentage slope method [13]. All these discrimination methods can be generally categorized into time-domain, frequency-domain, and intelligent methods.

Generally, attributed to the better capability of capturing the dynamic information inside the pulse signals, intelligent methods tend to outperform time-domain as well as frequency-domain methods regarding the discrimination performance, but are more time-consuming due to the matrix computation and training they require. Recently, Liu et al. proposed a pulse-coupled neural network (PCNN)-based discrimination method that performs exceptionally well and exhibits comparable time consumption levels to time-domain methods [14]. Their work demonstrated the outstanding discrimination and anti-noise abilities of the PCNN when applied to the PSD. However, this algorithm requires several manually set parameters, which can affect its performance.

☆ This work was supported by the National Natural Science Foundation of China (Nos: 42104174, 12205078).
* Corresponding author. Chengdu University, Chengdu, 610106, China.
E-mail address: liubingqi@cdu.edu.cn (B.-Q. Liu).

https://doi.org/10.1016/j.net.2023.04.032

To solve this problem, we introduce the spiking cortical model (SCM) into the n-γ discrimination field, which is a simplified PCNN model. It is derived from the PCNN and has much fewer parameters as well as improved computational complexity and discrimination performance. To demonstrate the discrimination effect of the proposed method, experiments were conducted on the data of an n-γ superposed field, which is retrieved by a plastic scintillator (EJ299-33) and a digital oscilloscope (TPS2000B). This signal retrieve equipment was set with a bandwidth of 200 MHz, a sampling rate of 1 *GS/s*, a trigger threshold of 500 *mV* and a 160 *ns* pulse duration which does not bury the information inside signal respecting the Shannon criteria [15]. The experimental results of our proposed method were compared with the other methods, which are the PCNN, charge comparison, and zero-crossing. Subsequently, we elucidated the relationship between the SCM's dynamic properties and its discrimination performance, analyzed the role of each parameter of SCM, and presented a detailed parameter selection strategy.

This study is organized as follows: First, the principles of all discrimination methods used in this work are presented in Section 2. Then, in Section 3, we illustrate the evaluation criteria used for n-γ discrimination. In Section 4, we conduct experiments and evaluate the experimental results of different discrimination methods, and discuss the role of each SCM parameter. Finally, we present our conclusions in Section 5.

2. Fundamentals of discrimination methods

2.1. Pulse-coupled neural network

Pulse-coupled neural network is a bio-inspired neural network based on Eckhorn's cortical model. It is derived from the research on interactions between cell assemblies in cat's primary visual cortex [16], introduced by Johnson et al., in 1994 for imaging processing [17,18]. Differ from common neuron networks (deep learning models), the PCNN does not need the pre-training process to form the relationship between input and output data. On the contrary, the PCNN works in a way that is like real biological neurons, using the change of action potentials when neurons receive stimuli to solve the problem of scene analysis [19]. PCNN has developed rapidly in the past few decades in the imaging processing areas, such as the feature extraction [17], image segmentation [18], pattern recognition [20], object recognition [21,22], and image shadow removal [23]. There are three major domains in the PCNN, which are the accepted, modulation, and pulse generator domains, and the accepted domain is further divided into two parts: link input (LI) and feedback input (FI). The FI makes a main contribution to the action potential of a neuron while the LI modulate it. When the action potential of a neuron exceeds its dynamic threshold, this neuron is activated, and a spike is generated. The mathematical expression are as follows [24]:

$$\boldsymbol{F}_{ij}[n] = e^{-\alpha_F}\boldsymbol{F}_{ij}[n-1] + V_F\sum_{kl}\boldsymbol{M}_{ijkl}\boldsymbol{Y}_{kl}[n-1] + \boldsymbol{S}_{ij} \tag{1}$$

$$\boldsymbol{L}_{ij}[n] = e^{-\alpha_L}\boldsymbol{L}_{ij}[n-1] + V_L\sum_{kl}\boldsymbol{W}_{ijkl}\boldsymbol{Y}_{kl}[n-1], \tag{2}$$

$$\boldsymbol{U}_{ij}[n] = \boldsymbol{F}_{ij}[n]\{1+\beta\boldsymbol{L}_{ij}[n]\}, \tag{3}$$

$$\boldsymbol{Y}_{ij}[n] = \begin{cases} 1, \boldsymbol{U}_{ij}[n] > \boldsymbol{\theta}_{ij}[n] \\ 0, \text{otherwise} \end{cases} \tag{4}$$

$$\boldsymbol{\theta}_{ij}[n] = e^{-\alpha_\theta}\boldsymbol{\theta}_{ij}[n-1] + V_\theta\boldsymbol{Y}_{ij}[n-1], \tag{5}$$

where the internal activity of a neuron located at the position (i,j) $\boldsymbol{U}_{ij}$ is determined by the feedback input $\boldsymbol{F}_{ij}$ and link input $\boldsymbol{L}_{ij}$, which are coupled by a factor named linking strength β. n is the iteration count. α_F and α_L denote the decay time constants of FI and LI, respectively. V_F and V_L represent the amplification coefficients of FI and LI, respectively. For a central neuron in the position (i,j), it is connected with neighboring neurons located at (k,l) through constant synaptic weight matrixes W and M. $\boldsymbol{S}_{ij}$ is the input stimulus. $\boldsymbol{\theta}_{ij}$ is the dynamic threshold of a neuron in the location (i,j), α_θ is the decay time constants of the dynamic threshold, and V_θ denotes the amplification coefficients of the dynamic threshold. $\boldsymbol{Y}_{ij}$ is the timing pulse sequence that determines whether a neuron located at (i,j) should be fired ($\boldsymbol{U}_{ij}[n] > \boldsymbol{\theta}_{ij}[n]$, $\boldsymbol{Y}_{ij}[n] = 1$) or not ($\boldsymbol{U}_{ij}[n] \le \boldsymbol{\theta}_{ij}[n]$, $\boldsymbol{Y}_{ij}[n] = 0$).

In [14], Liu et al. introduced the PCNN into the n-γ discrimination filed for the first time, demonstrating its capacity to capture the dynamic information inside the radiation pulse signals, which makes it capable of discriminating neutrons and gamma-rays pulse signals effectively. Feed the PCNN with a radiation pulse signal, an ignition map could be generated, which is a same size vector as the pulse signal. The ignition times of n-γ pulse signals are different in the falling edge and delayed fluorescence parts because of the intrinsic difference between their pulse shapes. By summing up the corresponding parts of the ignition map, the n-γ pulse signals can be separated. Besides, the integration of ignition times of gamma-ray signals is less than that of neutron signals.

2.2. Charge comparison

Charge comparison [25], as a widely used method in n-γ discrimination, is generally applied in many industrial fields attributed to its efficiency and stability of discrimination. This method is based on the different interaction features of neutrons and gamma-rays when they penetrate the sensitive volume of a radiation detector, i.e., the charge ratio R of a neutron is different from that of a gamma-ray photon. Subsequently, by calculating the charge ratio R, Hawkes et al. successfully discriminated n-γ pulse signals [26]. The formula of R is given as follows:

$$R = \frac{Q_N}{Q_M} \tag{6}$$

where Q_N represents the integration of the voltage of the slow component of a pulse signal, while Q_M is the integration of the voltage of the whole signal. Account to the longer decay time of the falling edge of the neutron signals as well as the delayed fluorescence of neutrons, the R-value of neutrons is larger compared with the gamma-rays.

2.3. Zero-crossing

In the Zero-crossing method [27,28], the pulse shape information is carried by a criterion called zero-crossing time, which can be calculated by transforming a neutron or gamma-ray pulse signal to a bipolar pulse. The time interval between the beginning of the bipolar pulse and the zero-crossing point of it is the zero-crossing time. With regard to the transformation to a bipolar pulse signal, M. Nakhostin [29] proposed a digital $CR - RC^2$ filter, the recursive form of which is derived from calculating the Z-transfer function of it. The recursive formula of the bipolar signal can be expressed as follows:

$$y[n] = 3\delta y[n-1] - 3\delta^2 y[n-2] + \delta^3 y[n-3] + T\delta\left(1 - \frac{\omega T}{2}\right)x[n-1] - T\delta^2\left(1 + \frac{\omega T}{2}\right)x[n-2] \tag{7}$$

where x is the pulse signal of neutron or gamma-ray, y denote the filtered pulse i.e., the bipolar signal, n represent the sample index, and δ and ω are constants decided by

$$\delta = e^{-T/\tau} \tag{8}$$

$$\omega = \frac{1}{\tau} \tag{9}$$

where T is the sampling interval of the pulse signal, and $\tau = RC$ represents the shaping time. 10% of the pulse maximum is set as the start time and the first sample after the pulse's peak that below zero is set as zero-crossing time. Since the falling edge of gamma-ray pulse signals is steeper than that of neutron pulse signals, the zero-crossing time of gamma-rays is shorter than neutrons.

2.4. Spiking cortical model

Zhang et al. (2018) introduced the spiking cortical model (SCM), a neural network model that is a derivative of the PCNN model [30]. SCM has an advantage over PCNN and other PCNN-derived methods such as the intersecting cortical model due to its characteristics of having fewer parameters, lower computational complexity, and higher accuracy. These advantages make it widely applicable in image processing areas such as image segmentation [31], where it has displayed excellent performance. Similar to biological neurons, the membrane potential of a neuron in SCM is calculated by a combination of direct stimulation and synaptic modulation exerted by neighboring neurons. When the membrane potential of a neuron surpasses its dynamic threshold, it generates a spike, which further affects neighboring neurons in the next iteration. The mathematical description of the SCM is given as follows:

$$\tilde{\boldsymbol{U}}_{ij}(n) = f\tilde{\boldsymbol{U}}_{ij}(n-1) + \tilde{\boldsymbol{S}}_{ij}\left(1 + \sum_{kl}\tilde{\boldsymbol{W}}_{ijkl}\tilde{\boldsymbol{Y}}_{kl}(n-1)\right) \tag{10}$$

$$\tilde{\boldsymbol{Y}}_{ij}(n) = \begin{cases} 1, if\ \dfrac{1}{1+\exp(-(\boldsymbol{U_{ij}}(n) - \boldsymbol{\theta}_{ij}(n)))} > 0.5 \\ 0, otherwise \end{cases} \tag{11}$$

$$\tilde{\boldsymbol{\Theta}}_{ij}(n) = g\tilde{\boldsymbol{\Theta}}_{ij}(n-1) + h\tilde{\boldsymbol{Y}}_{ij}(n) \tag{12}$$

where n represents the iteration count, $\tilde{\boldsymbol{U}}_{ij}(n)$ denotes the membrane potential of a neuron in the location (i,j) at iteration n, f is the attenuation constant of the membrane potential, $\tilde{\boldsymbol{S}}_{ij}$ represents the external stimulus, $\tilde{\boldsymbol{W}}_{ijkl}$ denotes the synaptic weight matrix which affects the connection between a neuron in location (i,j) and its neighboring neurons in location (k,l), $\tilde{\boldsymbol{Y}}$ stands for the output action potential (i.e. the output spike) of a neuron, the convolution of $\tilde{\boldsymbol{W}}_{ijkl}$ and $\tilde{\boldsymbol{Y}}_{kl}(n-1)$ represents the modulation on the central neuron located at (i,j) by its neighboring neurons in location (k,l), $\tilde{\boldsymbol{\Theta}}_{ij}$ is the dynamic threshold of a neuron in location (i,j), g and h are the attenuation constant of the threshold and the absolute refractory period respectively, which prevents neurons that just been activated from being reactivated immediately.

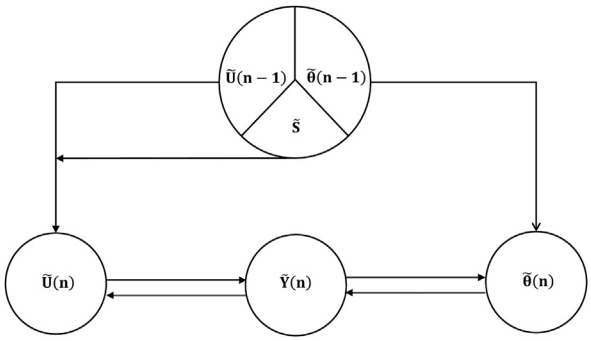

Fig. 1. Schematic of the spiking cortical model. The SCM has three essential components: the membrane potential $\tilde{\boldsymbol{U}}$, the output action potential $\tilde{\boldsymbol{Y}}$, and the dynamic threshold $\tilde{\boldsymbol{\Theta}}$, which are all closely interlinked; changes in any of these components affect the others. $\tilde{\boldsymbol{U}}$ and $\tilde{\boldsymbol{\Theta}}$ are partly decided by their values in the previous iteration, while $\tilde{\boldsymbol{U}}$ is also influenced by $\tilde{\boldsymbol{Y}}$ and $\tilde{\boldsymbol{S}}$. $\tilde{\boldsymbol{\Theta}}$ is modulated by $\tilde{\boldsymbol{Y}}$, while $\tilde{\boldsymbol{Y}}$ directly depends on the relative size of $\tilde{\boldsymbol{U}}$ and $\tilde{\boldsymbol{\Theta}}$.

Intuitively, as shown in Fig. 1, there are three important parts in the SCM: the membrane potential $\tilde{\boldsymbol{U}}$, the output action potential $\tilde{\boldsymbol{Y}}$, and the dynamic threshold $\tilde{\boldsymbol{\Theta}}$. These parts are closely connected, the changing of each of them will affect others. The potentials of $\tilde{\boldsymbol{U}}$ and $\tilde{\boldsymbol{\Theta}}$ are partly decided by the potentials of themselves in the last iteration respectively. Additionally, $\tilde{\boldsymbol{U}}$ is affected by $\tilde{\boldsymbol{Y}}$ and the external stimulus $\tilde{\boldsymbol{S}}$. On the other hand, $\tilde{\boldsymbol{\Theta}}$ is modulated by $\tilde{\boldsymbol{Y}}$, while $\tilde{\boldsymbol{Y}}$ directly depends on the size relationship between the membrane potential $\tilde{\boldsymbol{U}}$ and the dynamic threshold $\tilde{\boldsymbol{\Theta}}$.

According to the Weber-Fechner law [32], a psychophysics law that describes the human visual system, the subjective sense of the intensity $\tilde{I}$ is related to the time matrix $\tilde{T}$, with the human visual system being more sensitive to low intensity rather than high intensity. Fig. 2 illustrates the situation whereby the SCM receives a high-intensity stimulus and a low-intensity one. When comparing two intervals with equal thresholds, $\Delta\tilde{\theta}_1$ and $\Delta\tilde{\theta}_2$, it is evident that the processing time of a high-intensity stimulus Δt_1 is significantly shorter than that of a low-intensity stimulus Δt_2. This indicates that, similar to the human visual system, the SCM is also more sensitive to low intensity than to high intensity.

In 2021, Liu et al. validated the application of PCNN on n-γ

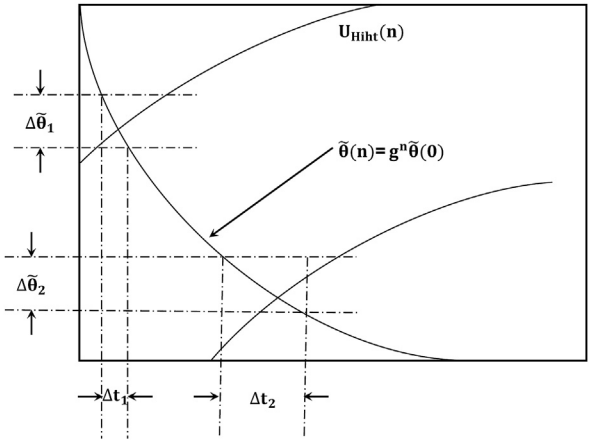

Fig. 2. Process of high intensity and low intensity of stimuli. For two equal threshold intervals $\Delta\theta_1$ and $\Delta\theta_2$, the processing time of high stimulus Δt_1 is much shorter than that of low stimulus Δt_2, indicating that the SCM is also more sensitive to low intensity rather than high intensity.

discrimination [14]. They found that the dynamic information inside the pulse signals can be effectively captured by the PCNN, which is extremely essential to its outstanding discrimination performance. When the SCM is applied to discriminate n-γ pulse signals, it processes the radiation pulse signals by generating an ignition map that shows the ignition counts of each pulse signal sampling point, as shown in Fig. 3. From these figures, it is evident that the primary difference between the shape of n-γ pulse signals is the steepness of the falling edge and whether there is delayed fluorescence. Specifically, the falling edge of gamma-ray is steeper than that of the neutron, and the delayed fluorescence is a unique characteristic of neutrons. These two differences can be distinguished by the SCM and are clearly magnified in the ignition map. By integrating the corresponding parts of the ignition map that contained the information of the falling edge and the delayed fluorescence, the n-γ pulse signals can be accurately discriminated. Note that the integration of neutrons is larger than that of gamma-rays.

3. Evaluation criteria

To analyze the results of different n-γ discrimination methods, two objective discrimination measures are utilized in this work, which are the figure of merit (*FoM*) and the time consumption of discrimination (discrimination time, defined as the CPU time required to discriminate all radiation pulse signals). To calculate the *FoM*-value, the histogram of n-γ counts need to be drawn, and then a Gaussian fitting function is used to form the curves of the neutrons and gamma-rays, as shown in Fig. 4. The *FoM* is defined as [33]:

$$FoM = \frac{S}{FWHM_n + FWHM_\gamma} \tag{16}$$

where the distance between two peaks of the neutrons and gamma-rays is denoted by *S*, the full width at half maximum of neutron and gamma-ray curves are represented by $FWHM_n$ and $FWHM_\gamma$, respectively. A shorter discrimination time and a larger *FoM*-value indicate a better discrimination performance.

4. Experiment

4.1. Discrimination results

4.1.1. Parameter settings

The optimized values of parameters of the PCNN are: $n = 180$, $\alpha_F = 0.32$, $\alpha_L = 0.356$, $\alpha_\theta = 0.08$, $V_F = 0.0005$, $V_L = 0.0005$, $V_\theta = 15$, $\boldsymbol{M} = \boldsymbol{N} = [0.1409, 0, 0.1409]$, $\beta = 0.67$. The integration interval of an ignition map is selected as between 10 *ns* before the peak of a pulse signal and 120 *ns* after it.

Regarding the charge comparison method, the total component is selected between 15 *ns* before the peak of a pulse signal and 200 *ns* after it, and the slow component is composed of an interval between 7 *ns* before and 200 *ns* after the peak of a pulse signal.

For the zero-crossing method, $T = 1$ *ns* and $\tau = 72$ *ns*.

The parameters of the SCM are set as: $n = 36$, $f = 0.8$, $g = 0.704$, $h = 18.2$, $\bar{\boldsymbol{W}} = [0.44, 0, 0.44]$.The interval between 5 *ns* before the peak of a pulse signal and 125 *ns* after the peak of a pulse signal is selected as the integration interval of an ignition map.

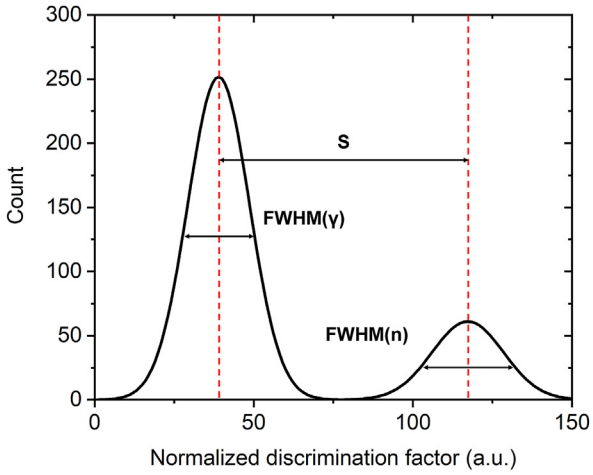

Fig. 4. n-γ discrimination evaluation criteria. The evaluation criteria *FoM*-value is calculated by Eq. (16), comprising of three parts that are shown in this figure (*S*, $FWHM_n$, and $FWHM_\gamma$). A larger *FoM*-value indicate a better discrimination performance.

4.1.2. Experimental results evaluation

In this work, a ^{241}Am–Be isotope neutron source whose average energy is 4.5 *MeV* is used to generate the neutrons and gamma-ray superposed field. The radiation pulse signals are retrieved by a plastic scintillator (EJ299-33) and a digital oscilloscope (TPS2000B), which was set with a bandwidth of 200 MHz, a sampling rate of 1 *GS/s*, a 160 *ns* pulse duration, and a trigger threshold of 500 *mV*, corresponding to an energy of 1.6 *MeVee* approximately (the definition of *MeVee* is given in Ref. [14]). Based on this setup, 9414 n-γ pulse signals are retrieved, the pulses shape of which are drawn in Fig. 3A. Clearly, the luminous attenuation rate of the neutron is distinctly slower compared with the gamma-rays, accounting for the longer decay time of neutrons and the unique characteristic

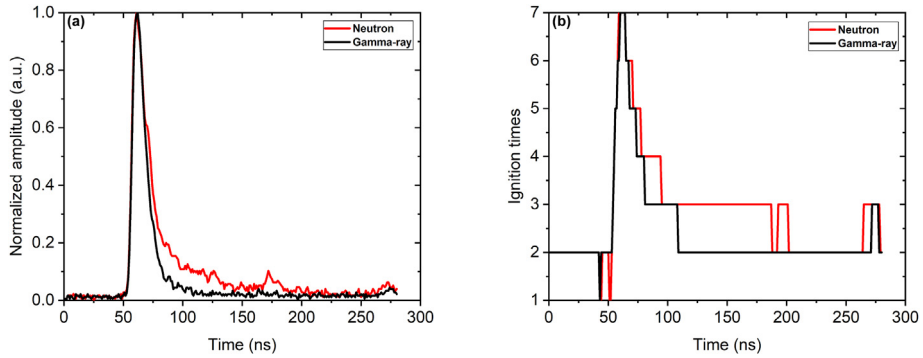

Fig. 3. Comparison of normalized n–γ pulses and their ignition maps. (a) The n-γ pulse signals. (b) The ignition maps of n-γ pulse signals, which are generated by implementing SCM on the n-γ pulse signals. The difference between neutron and gamma-ray in (a) can be distinguished by the SCM and are significantly magnified in the ignition map (b), showing that the inherent differences between n-γ pulses in the falling edge and the delayed fluorescence are successfully captured by the SCM.

that neutron has, the delayed fluorescence [34].

Before the discrimination process, all n-γ pulse signals need to be filtered by the Fourier transform [35] to reduce the noise. Notice that there are many different filtering methods in the n-γ discrimination fields such as wavelet transform [36,37], Kalman filter [38], and sliding average filter [39], and different filtering methods coupled with different discrimination methods could exhibit different discrimination performance [12,40]. Because the main discussion topic in this work is irrelevant to the filtering methods, we chose the most commonly used filtering method, the Fourier transform, to apply to all discrimination methods used in this study. Then, the filtered n-γ pulse signals can be discriminated by four methods mentioned in Sect.2, processed on an AMD R9-5900X CPU. The results are given in Fig. 5.

Fig. 5a is the scatter plot of the pulse signals counts of neutrons and gamma-rays, discriminated by the aforementioned four discrimination methods, where discrimination results of the n-γ pulse signals are divided into two groups of dots by a crossing line, the dots below it are recognized as the gamma-ray signals and the dots above it are recognized as the neutron signals. Notice that the discrimination factors of different discrimination methods are normalized to the range 0–40, whereas there are a few signals that deviated from the Neutron counts group too far away in the results of Charge comparison method; hence we move the range of the Charge comparison method from range 0–40 to approximately range 10–50, aiming to achieve a universal crossing line that can cross over the gaps between neutron and gamma-ray groups of all discrimination methods. For the situation of good discrimination performance, the group of gamma-ray dots and the grout of neutron dots should be as separated from each other as possible, and each group should be distributed centrally while exhibiting a clear Gaussian distribution at the same time. It is noted that the performances of the PCNN and SCM significantly outperform that of the zero-crossing method and charge comparison method, with a clear gap between the groups of neutrons and gamma-rays. Besides, the group of dots of n-γ pulse signals counts of these two methods are distributed noticeably centralized and maintain the characteristic of Gaussian distribution, with very few discrete dots between the two groups or on the outside.

Fig. 5b shows the Gaussian fitting of the histograms of the discrimination results of different methods, which are used to calculate the *FoM*-value of each method. Furthermore, they provide an intuitive view of the discrimination performance. A good discrimination effect is characterized by (i) a wide gap between two bands, and (ii) a narrow FWHM. It is necessary to mention that the discrimination factor generated by each method used to create the histogram varies due to internal principles, leading to different histogram bin counts and thus varying Y-axis values. However, Y-axis values are irrelevant to the discrimination effect and are only a byproduct used to present all method results in one figure. Analysis of the figure reveals that the discrimination effect of the PCNN and SCM is noticeably better than that of other methods, with clear, wide gaps between their bands and narrow FWHM widths.

To further tell the difference between the performance of the PCNN and SCM, objective evaluation criteria are needed. The *FoM*-value of every method was calculated and presented in Table 1, along with the discrimination time (the total time consumption of processing the 9414 pulse signals) of each of them. The neutron and gamma-ray counts of each discrimination method are also provided to demonstrate that pulse signals were not wrongly discriminated because the signal categorization results are generally consistent throughout all discrimination methodologies.

As shown in Table 1, it is consistent with the subjective evaluation results made by using Fig. 5 that the discrimination performance of the PCNN and SCM is significantly better than that of zero-crossing method and charge comparison method, with clearly larger *FoM*-values. The discrimination effect of the SCM outperforms that of the others, which has a 34.81% improvement in the *FoM*-value and an outstanding 75.67% improvement in the discrimination time compared with the PCNN method, a significant 50.29% improvement in the *FoM*-value and 70.65% improvement in the discrimination time compared with the charge comparison method, and an excellent 110.02% improvement in the *FoM*-value and 38.4% longer discrimination time compared with the zero-crossing method. This astonishing performance is attributed to the accuracy and computational improvement of the SCM compared with the PCNN model on the one hand. And on the other, their iteration counts of them are different which have a great effect on the time consumption of discrimination. Although the PCNN model performs well when it is applied to the two-dimensional image processing, its complex design makes it needs more iteration count to capture the information contained in the data fed to it, while the SCM, as a simplified model, needs much less iteration count especially when the data it needs to process is a one-dimensional matrix like a radiation pulse signal.

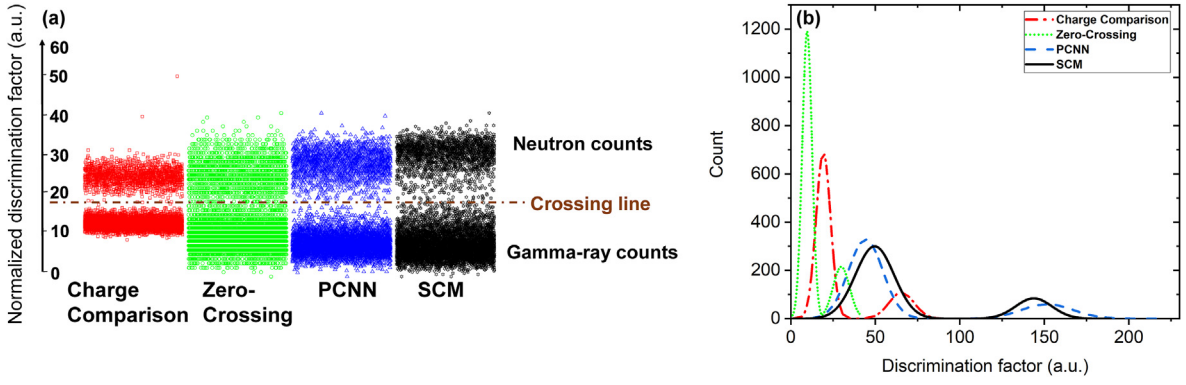

Fig. 5. The discrimination results. (a) Scatter plot of the discrimination results of four methods. The discrimination results of the n-γ pulse signals are divided into two groups of dots by a crossing line, the dots below it are recognized as the gamma-ray signals and the dots above it are recognized as the neutron signals. For the situation of fine discrimination performance, the group of gamma-ray dots and the grout of neutron dots should be as separated from each other as possible, and each group should be distributed centrally while exhibiting a clear Gaussian distribution at the same time. (b) Gauss fitting curves for the histogram of different discrimination methods. The histogram is used to calculate the *FoM*-value of each method, while it can also give an intuitive view of the discrimination performance. A good discrimination effect holds two characteristics: (i) a wide gap between two bands, and (ii) the full-width at half-maximum of each band is narrow.

Table 1
Discrimination results and evaluation.

Discrimination method	PCNN	Charge comparison	Zero-crossing	SCM
Discrimination time	2.22 s	1.84 s	**0.39 s**	0.54 s
Discrimination effect (*FoM*)	1.709	1.533	1.097	**2.304**
Neutron count	2056	2092	2742	2071
Gamma-ray count	7358	7322	6672	7343

4.2. Parameters of the SCM

Compared with the PCNN, the number of parameters of the SCM is much lesser, but these parameters still affect the discrimination performance. Consequently, the discussion of the parameter selection scheme is necessary. The variation curve of the *FoM*-value when one parameter is changed while others remain the values mentioned in Sec. 4.1.1 is drawn in Fig. 6.

As shown in Fig. 6, by selecting appropriate parameters, the *FoM*-value can be easily stabilized between 1.5 and 2.3, indicating that the SCM does not heavily rely on parameter settings to achieve a good discrimination performance. For the iteration count n, as shown in Fig. 6a, the variation curve of the *FoM*-value by it shows obvious periodic fluctuation, and the peak value of the fluctuation curve is greater when the number of iterations is lower. The reason for such a pattern is that with the increase of iterations, the general action potential of each neuron is initially climbing and then inclined to stabilization, which means the action potential is more dependent on the external stimuli firstly and then becomes more dependent on the neurons' action potentials in former iterations. Regarding the n-γ discrimination, the information contained in the external stimuli is more important and the modulation of affection from potential in its last iteration should be not too large, hence the small value of the iteration count should be taken. For the attenuation constant of the threshold g, as shown in Fig. 6b, which decides the attenuation speed of the threshold and affect the frequency of activation of a neuron, the variation curve of the *FoM*-value by it also exhibits a pattern of periodic fluctuation, the value of it can be chosen at the peaks of the curve. For the attenuation constant of the membrane potential f, as shown in Fig. 6c, there is an optimal range of values around 0.8. f controls the attenuation speed of the membrane potential of a neuron, if the value of it is too large, the contribution of the potential comes from the last iteration would be too little, and vice versa. Consequently, an optimal range of f is in the middle.

For the synaptic weight matrix $\tilde{\boldsymbol{W}}$, as shown in Fig. 6d, which controls the connection between the central neuron and its neighbors, the variation curve of the *FoM*-value by it has an overall tendency to decline when the value of $\tilde{\boldsymbol{W}}$ is too far from 0.44. The value of $\tilde{\boldsymbol{W}}$ has a large effect on the contribution of the membrane potential $\boldsymbol{U}$ by neighboring neurons, which decides the proportion of external stimuli in $\boldsymbol{U}$. As we have mentioned before, the contribution of external stimuli $\boldsymbol{S}$ is very important to the n-γ discrimination and it needs to be dominant in $\boldsymbol{U}$, and although the modulation of the neighboring neurons is also important to the information retrieving of SCM, the level of modulation should not be too large to over the external stimuli nor too little to abandon the effect of modulation, so the performance is good when the value of $\tilde{W}$ locates in the middle. Finally, for the absolute refractory period h, as shown in Fig. 6f, the variation curve of the *FoM*-value by it rises drastically at the first and then tends to be stable after 18. This parameter decides the characteristic of dynamic threshold $\tilde{\boldsymbol{\Theta}}$, which makes an activated neuron not be activated again immediately, the value of it should be selected larger in a reasonable range.

In general, the variation curve of the *FoM*-value by many parameters shows periodic fluctuation in a reasonable range and the

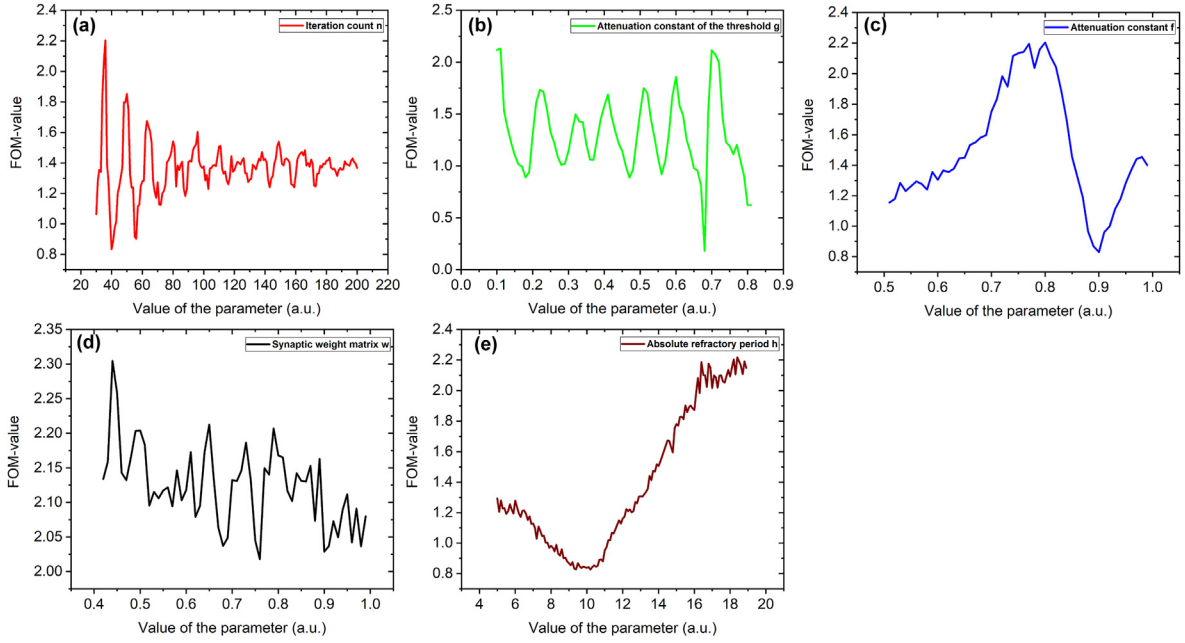

Fig. 6. The variation curve of the *FoM*-value by different parameters. In general, the variation curve of the *FoM*-value by many parameters shows periodic fluctuation in a reasonable range and the performance of discrimination would be very bad when the parameters are selected too extreme and out of the reasonable range.

performance of discrimination would be very bad when the parameters are selected too extreme and out of the reasonable range. The reason for this appearance is that different parts of the SCM are closely connected, if the characteristic of one-part changes too far, it would affect others and cause others to modulate this part to work properly, which leads to the periodic fluctuation. However, when the value of a parameter is too extreme to maintain the connected and mutually modulated relationship between different parts of the SCM, the discrimination performance of the SCM would decline dramatically. The appropriate parameters of the SCM can be selected by using the above parameter change pattern to achieve a good n-γ discrimination performance.

5. Conclusion

This study proposed the SCM-based neutrons and gamma-rays discrimination method and compares it with three other methods: the pulse-coupled neural network (PCNN), charge comparison and zero-crossing. The radiation pulse signals from a neutron and gamma-ray superposed field used in our work were generated by a ^{241}Am–Be isotope neutron source, detected by a plastic scintillator (EJ299-33), and processed on an AMD R9-5900X CPU. The experimental results demonstrated that the proposed method exhibits exceptional discrimination performance and outperforms the others. Specifically, it delivers the highest *FoM*-value (34.81% improvement compared with the PCNN, 70.54% improvement compared with the charge comparison, and 110.02% improvement compared with the zero-crossing) and the second-fastest discrimination time (75.67% improvement compared with the PCNN, 59.95% improvement compared with the charge comparison, and 38.4% slower than the zero-crossing). The SCM's breakthrough discrimination performance is due to its capability to recognize dynamic information in pulse signals - a crucial metric for neutrons and gamma-rays discrimination. This performance is enhanced by its improved accuracy and computational complexity compared to the PCNN. The SCM's excellent discrimination effect makes it applicable to many fields requiring accurate discrimination of neutrons and gamma-rays, while its improved discrimination time demonstrates its potential to be used in real-time discrimination scenarios. Thus, the SCM method has the potential to enable high-quality real-time discrimination, similar to the zero-crossing method.

In addition, the influence pattern of each parameter on the SCM and the reason that caused this pattern are discussed. The variation curve of the *FoM*-value by many parameters shows periodic fluctuation if the value of the parameter is in a reasonable range, but if not, the discrimination performance would noticeably decrease, attributable to the interconnected and mutually modulated relationship between different SCM parts. In our future work, we will further research the SCM parameters with the aim of designing an auto-setting SCM model for the n-γ discrimination.

Author contributions

All authors contributed to the study conception and design. Material preparation, data collection and analysis were performed by Hao-Ran Liu and Bing-Qi Liu. The first draft of the manuscript was written by Hao-Ran Liu, and all authors commented on previous versions of the manuscript. All authors read and approved the final manuscript.

Declaration of competing interest

The authors declare that they have no known competing financial interests or personal relationships that could have appeared to influence the work reported in this paper.

References

[1] Lei Wang, Josh Jarrell, Sha Xue, et al., Fast neutron detection at near-core location of a research reactor with a SiC detector, Detect. Assoc. Equip. 888 (2018) 126–131, https://doi.org/10.1016/j.nima.2018.01.070.

[2] G. Tosi, A. Torresin, S. Agosteo, et al., Neutron measurements around medical electron accelerators by active and passive detection techniques, Med. Phys. 18 (1) (1991) 54, https://doi.org/10.1118/1.596751.

[3] A. El-Taher, Rare earth elements content in geological samples from eastern desert, Egypt, determined by instrumental neutron activation analysis, Appl. Radiat. Isot. 68 (9) (2010) 1859–1863, https://doi.org/10.1016/j.apradiso.2010.02.012.

[4] L.R. Greenwood, R.R. Heinrich, R.J. Kennerley, et al., Development and testing of neutron dosimetry techniques for accelerator-based irradiation facilities, Nucl. Technol. 41 (1) (1978) 109–128, https://doi.org/10.13182/NT78-A32137.

[5] M.L. Litvak, I.G. Mitrofanov, A.B. Sanin, et al., LEND neutron data processing for the mapping of the Moon, J. Geophys. Res. 117 (2012) E00H32, https://doi.org/10.1029/2011JE004035.

[6] F.D. Brooks, Development of organic scintillators, Nucl. Instrum. Methods 162 (1–3) (1979) 477–505, https://doi.org/10.1016/0029-554X(79)90729-8.

[7] D. Cester, M. Lunardon, G. Nebbia, et al., Pulse shape discrimination with fast digitizers, Nucl. Instrum. Meth. Phys. A 748 (2014) 33–38, https://doi.org/10.1016/j.nima.2014.02.032.

[8] M.L. Roush, M.A. Wilson, W.F. Hornyak, Pulse shape discrimination, Nucl. Instrum. Methods 31 (1) (1964) 112–124, https://doi.org/10.1016/0029-554X(64)90333-7.

[9] C. Frangville, A. Grabowski, J. Dumazert, et al., Nanoparticles-loaded plastic scintillators for fast/thermal neutrons/gamma discrimination: simulation and results, Nucl. Instrum. Meth. Phys. A942 (2019), 162370, https://doi.org/10.1016/j.nima.2019.162370.

[10] R. Coulon, V. Kondrasovs, Q. Lecomte, et al., Multilayer phoswich scintillators for neutron/gamma discrimination, Radiat. Meas. 117 (2018) 57–62, https://doi.org/10.1016/j.radmeas.2018.07.011.

[11] D. Wolski, M. Moszyński, T. Ludziejewski, et al., Comparison of n-c discrimination by zero-crossing and digital charge comparison methods, Nucl. Instrum. Methds Phys. Res. Sect. A Accel. Spectrom. Detect Assoc. Equip. 360 (3) (1995) 584–592, https://doi.org/10.1016/0168-9002(95)00037-2.

[12] Z. Zuo, H.R. Liu, Y.C. Yan, et al., Adaptability of n–c discrimination and filtering methods based on plastic scintillation, Nucl. Sci. Tech. 32 (2021) 28, https://doi.org/10.1007/s41365-021-00865-3.

[13] Zhuo Zuo, YuLong Xiao, ZhenFeng Liu, et al., Discrimination of neutrons and gamma-rays in plastic scintillator based on falling-edge percentage slope method, Nucl. Instrum. Methods Phys. Res. Sect. A Accel. Spectrom. Detect. Assoc. Equip. 1010 (2021), 165483, https://doi.org/10.1016/j.nima.2021.165483.

[14] H.R. Liu, Y.X. Cheng, Z. Zuo, et al., Discrimination of neutrons and gamma rays in plastic scintillator based on pulse-coupled neural network, Nucl. Sci. Tech. 32 (2021) 82, https://doi.org/10.1007/s41365-021-00915-w.

[15] J. Iwanowska-Hanke, M. Moszynski, L. Swiderski, et al., Comparative study of large samples (2"x2") plastic scintillators and EJ309 liquid with pulse shape discrimination (PSD) capabilities, J. Instrum. 9 (6) (2014), P06014, https://doi.org/10.1088/1748-0221/9/06/P06014.

[16] R. Eckhorn, H.J. Reitboeck, M. Arndt, et al., Feature linking via synchronization among distributed assemblies: simulations of results from cat visual cortex, Neural Comput. 2 (3) (1990) 293–307, https://doi.org/10.1162/neco.1990.2.3.293.

[17] J. Johnson, Pulse-coupled neural nets: translation, rotation, scale, distortion, and intensity signal invariance for images, Appl. Opt. 33 (1994) 6239–6253, https://doi.org/10.1364/AO.33.006239.

[18] H.S. Ranganath, G. Kuntimad, J.L. Johnson, Pulse Coupled Neural Networks for Image Processing, Proc. IEEE Southeastcon, Raleigh, NC, 1995, pp. 37–43, https://doi.org/10.1109/SECON.1995.513053.

[19] A.L. Hodgkin, A.F. Huxley, A quantitative description of membrane current and its application to conduction and excitation in nerve, J. Physiol. 117 (4) (1952) 500–544, https://doi.org/10.1113/jphysiol.1952.sp004764.

[20] K. Waldemark, T. Lindblad, V. Becanovic, et al., Patterns from the sky: satellite image analysis using pulse coupled neural networks for pre-processing, segmentation and edge detection, Pattern Recogn. Lett. 21 (3) (2000) 227–237, https://doi.org/10.1016/S0167-8655(99)00152-X.

[21] H.S. Ranganath, G. Kuntimad, Object detection using pulse coupled neural networks, IEEE Trans. Neural Network. 10 (3) (1999) 615–620, https://doi.org/10.1109/72.761720. May 1999.

[22] B. Yu, L. Zhang, Pulse-coupled neural networks for contour and motion matchings, IEEE Trans. Neural Network. 15 (5) (2004) 1186–1201, https://doi.org/10.1109/tnn.2004.832830.

[23] X. Gu, D. Yu, L. Zhang, Image shadow removal using pulse coupled neural network, IEEE Trans. Neural Network. 16 (3) (2005) 692–698, https://doi.org/10.1109/TNN.2005.844902.

[24] J.L. Johnson, M.L. Padgett, PCNN models and applications, IEEE Trans. Neural Network. 10 (3) (1999) 480–498, https://doi.org/10.1109/72.761706.

[25] D. Wolski, M. Moszyński, T. Ludziejewski, et al., Comparison of n-

discrimination by zero-crossing and digital charge comparison methods, Nucl. Instrum. Methds Phys. Res. Sect. A Accel. Spectrom. Detect Assoc. Equip. 360 (3) (1995) 584–592, https://doi.org/10.1016/0168-9002(95)00037-2.
[26] N.P. Hawkes, K.A.A. Gamage, G.C. Taylor, Digital approaches to field neutron spectrometry, Radiat. Meas. 45 (10) (2010) 1305–1308, https://doi.org/10.1016/j.radmeas.2010.06.043.
[27] P. Sperr, H. Spieler, M.R. Maier, et al., A simple pulse-shape discrimination circuit, Nucl. Instrum. Methods 116 (1974) 55, https://doi.org/10.1016/0029-554X(74)90578-3.
[28] S. Pai, W.F. Piel, D.B. Fossan, et al., A versatile electronic pulse-shape discriminator, Nucl. Instrum. Methods A278 (1989) 749, https://doi.org/10.1016/0168-9002(89)91199-6.
[29] M. Nakhostin, Recursive algorithms for real-time digital CR−(RC)n pulse shaping, IEEE Trans. Nucl. Sci. 58 (5) (2011) 2378–2381, https://doi.org/10.1109/TNS.2011.2164556.
[30] K. Zhan, H. Zhang, Y. Ma, New spiking cortical model for invariant texture retrieval and image processing. Neural Networks, IEEE Transactions on 12 (2009) 1980–1986, https://doi.org/10.1109/TNN.2009.2030585.
[31] K. Zhan, Jinhui Shi, Q. Li, J. Teng, M. Wang, Image Segmentation Using Fast Linking SCM, 2015 International Joint Conference on Neural Networks (IJCNN), 2015, https://doi.org/10.1109/ijcnn.2015.7280579.
[32] B.S. Manjunath, W.Y. Ma, Texture features for browsing and retrieval of image data, IEEE Trans. Pattern Anal. Mach. Intell. 18 (8) (1996) 837–842, https://doi.org/10.1109/34.531803.
[33] R.A. Winyard, J.E. Lutkin, G.W. McBeth, Pulse shape discrimination in inorganic and organic scintillators, I. Nucl. Instrum. Meth. 95 (1) (1971) 141–153, https://doi.org/10.1016/0029-554X(71)90054-1.
[34] B. D'Mellow, M.D. Aspinall, R.O. Mackin, et al., Digital discrimination of neutrons and c-rays in liquid scintillators using pulse gradient analysis, Nucl. Instrum. Meth. Phys. A 578 (1) (2007) 191–197, https://doi.org/10.1016/j.nima.2007.04.174.
[35] J. Allem, Short term spectral analysis, synthesis, and modification by discrete Fourier transform, IEEE Trans. Acoust. 25 (3) (1997) 235–238, https://doi.org/10.1109/TASSP.1977.1162950.
[36] S. Yousefi, L. Lucchese, M.D. Aspinall, Digital discrimination of neutrons and gamma-rays in liquid scintillators using wavelets, Nucl. Instrum. Methods A 598 (2009) 551–555, https://doi.org/10.1016/j.nima.2008.09.028.
[37] S. Hosur, A.H. Tewfik, Wavelet transform domain adaptive FIR filtering, IEEE Trans. Signal Process. 45 (1997) 617–630, https://doi.org/10.1109/78.558477.
[38] Y. Zheng, S. Chen, W. Tan, et al., Detection of tissue harmonic motion induced by ultrasonic radiation force using pulse-echo ultrasound and a Kalman filter, IEEE Trans. Ultrason. Ferroelectrics Freq. Control 54 (2007) 290–300, https://doi.org/10.1109/TUFFC.2007.243.
[39] J.A. Burns, E.M. Cliff, C. Rautenberg, A distributed parameter control approach to optimal filtering and smoothing with mobile sensor networks, in: 2009 17th Mediterranean Conference on Control and Automation, 2009, pp. 181–186, https://doi.org/10.1109/MED.2009.5164536.
[40] H. Liu, Z. Zuo, P. Li, B. Liu, L. Chang, Y. Yan, Anti-noise performance of the pulse coupled neural network applied in discrimination of neutron and gamma-ray, Nucl. Sci. Tech. 33 (2022) 75, 2022, https://doi:10.1007/s41365-022-01054-6.